# Fluid simulations of glow discharges: Effect of metastable atoms in argon

Dimitris P. Lymberopoulos and Demetre J. Economou[a)]
*Department of Chemical Engineering, Plasma Processing Laboratory, University of Houston, Houston, Texas 77204-4792*

(Received 9 October 1992; accepted for publication 23 December 1992)

A one-dimensional fluid simulation of a 13.56 MHz argon glow discharge including metastable species was performed as an example of a coupled glow-discharge/neutral-transport-reaction system. Due to the slow response time of metastables ($\sim 10$ ms) direct time integration of the coupled system requires $\sim 10^5$ rf cycles to converge. This translates to prohibitively long computation time. An "acceleration" scheme was employed using the Newton–Raphson method to speed up convergence, thereby reducing the computation time by orders of magnitude. For a pressure of 1 Torr, metastables were found to play a major role in the discharge despite the fact that their mole fraction was less than $10^{-5}$. In particular, metastable (two-step) ionization was the main mechanism for electron production to sustain the discharge. Bulk electric field and electron energy were lower, and a smaller fraction of power was dissipated in the bulk plasma when compared to the case without metastables. These results suggest that neutral transport and reaction must be considered in a self-consistent manner in glow discharge simulations, even in noble gas discharges.

## I. INTRODUCTION

Etching and deposition of thin films using low-pressure nonequilibrium gas discharges are crucial unit operations for fabrication of advanced microelectronic devices.[1] In plasma processing, feedstock gases are dissociated at near room temperature by high energy plasma electrons to produce reactive radicals and other intermediates. The reactive species interact with the semiconductor wafer to yield volatile products (etching) or to grow a solid film (deposition). The gas-solid reactions are strongly modified by energetic particle (mainly ion) bombardment. Control of the flux and energy distribution of the particles bombarding the wafer is essential for controlling etching or deposition rate, uniformity, selectivity, and etched feature wall profiles.

During the past decade there has been growing interest in modeling and simulation of reactive plasma processes.[2] Models range from the microscopic feature scale[3] to the wafer or plasma reactor scale.[4] Plasma reactor models focus either on the transport and reaction of radicals[5–7] (neutral transport and reaction models) or on the glow discharge physics (glow discharge models).[8–29] In the former case, the plasma is simply taken as a source of reactive radicals. Transport of charged particles is not treated or is handled in a rudimentary manner. The neutral transport and reaction models can easily handle complicated neutral chemistry and complex multidimensional geometries. However, the electron density and energy which are crucial for calculating the production rate of radicals, as well as the ion bombardment flux and energy, have to be estimated. In the glow discharge models, the charged particle densities, electron energy, and potential distribution are calculated as a function of time in the period of the applied field and space in the reactor. Derived quantities such as ionization and excitation rates, electron and ion current densities, and power deposition are also calculated. In these models emphasis is placed on the discharge physics neglecting neutral reactions. The ultimate goal is to couple the glow discharge with the neutral transport and reaction models into a global plasma reactor model (at least two dimensional) with predictive capabilities. The work of Sommerer and Kushner[30] is a solid step towards achieving this goal.

The glow discharge problem is very demanding computationally. Therefore, significant effort is expended in developing suitable numerical algorithms which capture steep gradients and provide convergent solutions in as short time as possible.[17,27,29,30] The vast majority of simulations are in one spatial dimension for dc or rf systems[8–12,18–30] and do not include neutral transport and reaction except for Ref. 30. Some two-dimensional dc[13,14] and rf[15] simulations have also been reported. These studies do not consider neutral transport and reaction.

Two kinds of glow discharge simulations are popular: fluid and kinetic simulations. In fluid simulations, moments of the Boltzmann equation are coupled to the Poisson equation to calculate the density, drift velocity, and energy of charged species and the self-consistent electric field. In the single moment approximation, the continuity equations for the charged species are solved together with the Poisson equation.[13–15,19] The drift/diffusion approximation is used instead of the momentum equations and the local field approximation is used instead of the electron energy balance. In the single moment approximation one assumes that the electron and ion momentum and energy relax to the equilibrium state on a time scale much shorter than the period of the applied field. In the two-moment approximation, an electron energy equation is added, removing the local field assumption.[8–12] Some workers have used an effective field to which the heavy ions respond.[11] In the three moment approximation, momentum balance

[a)]Author to whom correspondence should be addressed.

 0021-8979/93/083668-12$06.00  

equations are added to the density and energy continuity equations.[21] A comparison of the one-, two-, and three-moment approach has been reported by Li and Wu[31] for He gas. They also compared the fluid simulation results to a kinetic Monte Carlo simulation. The main advantage of fluid simulations is that they can be computationally efficient. However, the electron energy distribution function is not computed in a self-consistent manner. Therefore care must be exercised in calculating the electron transport properties and especially the electron reaction coefficients in the space and time varying field.[32]

Kinetic simulations employ the Boltzmann transport equation or Monte Carlo techniques and are capable of resolving the electron energy distribution function (eedf). The Boltzmann equation has been solved directly as for example in the convective scheme[33] or the phase-space particles motion scheme.[34] Earlier Monte Carlo studies used an assumed electric field.[35] Recently, particle in cell (PIC) methods coupled with Monte Carlo techniques to account for collisions have been used to resolve both the eedf and the ion distribution function.[18,36–38] All these simulations must consider Poisson's equation for the electrostatic field (or Maxwell's equations in general for the electromagnetic fields) to arrive at a self-consistent description of the discharge.

Kinetic simulations can resolve the spatiotemporal variations of the particle distribution functions, but have the disadvantage of long computation time especially at high pressure (high collision frequency) and/or when many particle reactions are taken into account. Fluid simulations are robust and computationally efficient but do not resolve the particle distribution functions. Hybrid fluid/kinetic models capitalize on the advantages of each method while at the same time they try to minimize the computation time.[28,30]

Most glow discharge models reported to date neglect neutral chemistry because of the disparate time scales involved. For instance, electrons respond on a nanosecond time scale while neutral reactions can happen on time scales of 100 s of milliseconds. It is therefore, customary to neglect neutral species reactions and calculate the electron density and energy based on the feedstock gas composition. However, the plasma gas composition can be very different than the feedstock gas composition. For example, molecular gases dissociate in the plasma to yield atoms and free radicals. These species can alter the electron properties when present even in small quantities. Another notable example is noble gas discharges which form long-lived metastable atoms. These metastables can affect the eedf and in turn the discharge characteristics even at mole fractions of $10^{-5}$. Very recently, Sommerer and Kushner[30] reported a hybrid fluid/Monte Carlo model of a one-dimensional rf discharge in He, $O_2$, or $SiH_4/NH_3$ including rather comprehensive plasma and neutral chemistry. Makabe *et al.*[39] reported a fluid simulation of an argon discharge including continuity equations for metastables and other excited states of argon. However, the neutral species continuity equations were decoupled from the charged particle density balance. This approach neglects the effect of metastable atoms on the ionization balance through stepwise ionization and metastable pooling reactions. Hence the effect of metastable species on the discharge properties could not be studied.

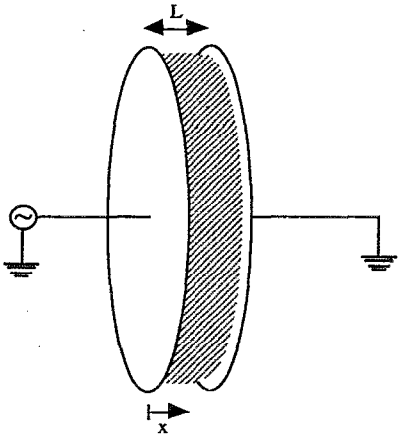


FIG. 1. Schematic of the parallel-plate discharge configuration.

In the present work, a fluid simulation of an argon discharge is reported including the effect of metastables. The metastable density balance is fully coupled to the charged species balance equations. Due to the long time scale of metastable species reactions, integration must be carried out for $\sim 10^5$ rf cycles to achieve convergence. An algorithm based on the Newton–Raphson method has been employed to speed up convergence by orders of magnitude. It is shown that metastables play an important role in the discharge at a pressure of $\sim 1$ Torr.

In Sec. II the model assumptions are outlined and model equations are presented. The method of solution is given in Sec. III. Section IV contains results and discussion. Conclusions are given in Sec. V.

## II. MODEL FORMULATION

A schematic of the glow discharge system modeled is shown in Fig. 1. The basic assumptions of the model are as follows:

(1) The discharge is formed between two large-area parallel conductive electrodes: discharge properties change along the direction normal to the electrodes only (i.e., $x$ axis).

(2) The particle flux is described by the diffusion/drift approximation and the effect of convective gas flow is negligible. Convective gas flow will not be an important factor when the gas residence time is much longer than the particle diffusion or reaction time. For a gas pressure $\sim 1$ Torr, flow rate $\sim 25$ sccm, and discharge volume $\sim 200$ cm$^3$, the gas residence time is $\sim 600$ ms. This is much longer than the metastable diffusion time of $\sim 10$ ms. Calculations for electrons and ions give even more conservative estimates. Of course, flow can affect the gas temperature but such complications are not considered in this work.

TABLE I. Important collision processes in argon discharge.

| No. | Process | Reaction | $H_j$ (eV) | Rate coefficient[a] | Ref. |
|---|---|---|---|---|---|
| 1 | Ground state excitation | $Ar+e\rightarrow Ar^*+e$ | 11.56 | $k_{ex}$ | 40 |
| 2 | Ground state ionization | $Ar+e\rightarrow Ar^+ +2e$ | 15.7 | $k_i$ | 40 |
| 3 | Step-wise ionization | $Ar^*+e\rightarrow Ar^+ +2e$ | 4.14 | $k_{si}$ | 40 |
| 4 | Superelastic collisions | $Ar^*+e\rightarrow Ar+e$ | −11.56 | $k_{sc}$ | 40 |
| 5 | Quenching to resonant | $Ar^*+e\rightarrow Ar^r+e$ | ⋯ | $k_r=2\times10^{-7}$ | 48–50 |
| 6 | Metastable pooling | $Ar^*+Ar,^*\rightarrow Ar^+ +Ar+e$ | ⋯ | $k_{mp}=6.2\times10^{-10}$ | 48–50 |
| 7 | Two-body quenching | $Ar^*+Ar\rightarrow 2Ar$ | ⋯ | $k_{2q}=3\times10^{-15}$ | 48–50 |
| 8 | Three-body quenching | $Ar^*+2Ar\rightarrow Ar_2+Ar$ | ⋯ | $k_{3q}=1.1\times10^{-31}$ | 48–50 |

[a]Rate coefficients for processes 1–4 are given as a function of electron energy in Fig. 2 (Ref. 40). Units are $cm^3/s$ except for $k_{3q}$ which is in $cm^6/s$.

(3) The electron energy distribution function (eedf) is not treated: an energy equation is solved for the electron "temperature" as if the eedf were Maxwellian. However, deviations from a Maxwellian distribution are accounted for when computing the rate coefficients of electron-particle reactions (see below).

(4) The particle diffusivity and mobility are constant for a given gas number density. Variable transport coefficients can be handled easily.

(5) Magnetic field effects are not included.

(6) Since ions are much heavier than electrons, ions can gain little energy from the applied field. In addition, ions can exchange energy efficiently in collisions with neutrals. Therefore the ion temperature is assumed constant and equal to the neutral temperature. An energy equation for the ions is, therefore, not needed.

(7) Molecular ions $Ar_2^+$ are neglected. An *a posteriori* estimate of the density of these ions (including production by three-body collision of $Ar^+$ with Ar neutrals, and loss by ion-electron recombination and ambipolar diffusion) showed that molecular ions are only 2% of the total ion density. Molecular ions are expected to become even less important at pressures below 1 Torr.

(8) Negative ions are neglected.

The continuity equations for electrons, positive ions, and metastable atoms are

$$\frac{\partial n_e}{\partial t}+\nabla\cdot\mathbf{J}_e=k_iNn_e+k_{si}n_*n_e+k_{mp}n_*^2, \tag{1}$$

$$\frac{\partial n_+}{\partial t}+\nabla\cdot\mathbf{J}_+=k_iNn_e+k_{si}n_*n_e+k_{mp}n_*^2, \tag{2}$$

$$\frac{\partial n_*}{\partial t}+\nabla\cdot\mathbf{J}_*=k_{ex}Nn_e-k_{si}n_*n_e-k_{sc}n_*n_e-k_rn_*n_e -2k_{mp}n_*^2-k_{2q}Nn_*-k_{3q}N^2n_*. \tag{3}$$

The particle fluxes are the superposition of drift under the influence of an electric field and diffusion in a concentration gradient. A drift term is not used for the metastables since these species are not charged

$$\mathbf{J}_e=-D_e\nabla n_e+\mu_e n_e\nabla V, \tag{4}$$

$$\mathbf{J}_+=-D_+\nabla n_+-\mu_+ n_+\nabla V, \tag{5}$$

$$\mathbf{J}_*=-D_*\nabla n_*. \tag{6}$$

The electron energy balance reads

$$\frac{\partial}{\partial t}\left(\frac{3}{2}n_ekT_e\right)+\nabla\cdot\mathbf{q}_e-e\mathbf{J}_e\cdot\nabla V+\sum_j H_jR_j=0 \tag{7}$$

with the total electron energy flux given by

$$\mathbf{q}_e=-K_e\nabla T_e+\tfrac{5}{2}kT_e\mathbf{J}_e, \tag{8}$$

where the thermal conductivity of electrons is given by $K_e=3/2kD_en_e$. Finally the Poisson equation relates the gradient of the local electric field to the charge density

$$\nabla^2V=-\frac{e}{\epsilon_0}(n_+-n_e). \tag{9}$$

In the above equations, $n_j$, $\mathbf{J}_j$, $D_j$, and $\mu_j$ $(j=e,+,*)$ are particle density, flux, diffusivity, and mobility, respectively. Subscripts $e$, $+$, and $*$ denote electrons, positive ions, and metastable atoms, respectively. $T_e$ is the electron "temperature," $V$ is the potential, and $\epsilon_0$ is the permittivity of free space. In Eq. (7), the summation is over all electron-neutral inelastic collisions. Energy loss in elastic collisions was found to be negligible. Table I shows collision processes, the corresponding rate coefficients, and the energy exchange per collision $H_i$. Positive values of $H_i$ imply energy loss by electrons (e.g., ionization) and negative values imply energy gain (superelastic collisions). In this analysis $n_*$ represents the density of a composite ($^3P_0$ and $^3P_2$) metastable level. Quenching of metastables by low energy electrons (reaction $R5$) creates the resonant states $^1P_1$ and $^3P_1$ (shown collectively as $Ar^r$ in Table I) which decay by emission of radiation. Stepwise ionization (reaction $R3$), and metastable pooling (reaction $R6$), couple the charged and neutral species transport/reaction processes. Finally, metastable quenching by argon ground states atoms in two- and three-body collisions are shown as reactions $R7$ and $R8$, respectively. Table I provides only a basic set of reactions for the argon discharge. A more complete set would include excitation and decay of higher states (e.g., $3p^54p$ states). A simplified spatially averaged model including higher states[40] revealed that the metastable density is not affected significantly, but the power balance can be affected.

The terms on the right hand side (rhs) of Eq. (1) are production of electrons by ionization of ground state argon atoms, metastable ionization (or step-wise ionization), and

TABLE II. Parameter values.

| Name | Symbol | Value | Reference |
|---|---|---|---|
| Electron diffusivity | $ND_e$ (cm s)$^{-1}$ | $3.86\times10^{22}$ | 51 |
| Positive ion diffusivity | $ND_+$ (cm s)$^{-1}$ | $2.07\times10^{18}$ | 47 |
| Metastable atom diffusivity | $ND*$ (cm s)$^{-1}$ | $2.42\times10^{18}$ | 52 |
| Electron mobility | $N\mu_e$ (V cm s)$^{-1}$ | $9.66\times10^{21}$ | 51 |
| Positive ion mobility | $N\mu_+$ (V cm s)$^{-1}$ | $4.65\times10^{19}$ | 51 |
| Secondary electron coefficient | $\gamma$ | 0.01 | ... |
| Electron temperature at wall | $T_{ec}=T_{ea}$ (eV) | 0.5 | ... |
| Electron recombination coefficient | $k_s$ | $1.19\times10^{7}$ cm/s | ... |

metastable-metastable destruction (pooling reactions), respectively. The terms on the rhs of Eq. (3) are production of metastables by electron impact excitation of ground state argon, and destruction of metastables by step-wise ionization, superelastic collisions with electrons, electron re-excitation to the resonant levels, metastable pooling, and metastable quenching, respectively. In the pristine argon discharge examined here the only quenching reactions considered are two- and three-body collisions with ground state argon atoms. Boundary conditions are as follows:

$$\mathbf{J}_e=\mp k_s n_e-\gamma\mathbf{J}_+ \quad @x=0,L, \tag{10}$$

$$\mathbf{J}_+=-\mu_+ n_+\nabla V \quad @x=0,L, \tag{11}$$

$$n_*=0 \quad @x=0,L, \tag{12}$$

$$T_e=0.5 \quad @x=0,L, \tag{13}$$

$$V=V_{\rm rf}\sin(2\pi ft) \quad @x=0,$$

$$V=0 \quad @x=L. \tag{14}$$

Here $k_s$ is the electron surface recombination coefficient calculated assuming an electron sticking coefficient of unity, $\gamma$ is the secondary electron emission coefficient, $V_{\rm rf}$ is the peak rf voltage, and $L$ is the interelectrode spacing. The boundary condition on electron temperature is difficult to specify.[8,9] A constant temperature $T_{ec}=T_{ea}=0.5$ eV was used in the present study. Tests using a temperature of 1 eV at the walls showed that the bulk plasma is not affected, but the time-average electron temperature at the plasma/sheath interface increases slightly. Parameter values are shown in Table II.

The initial conditions were

$$n_e=n_+=n_*=10^7+10^9(1-x/L)^2(x/L)^2, \quad \text{cm}^{-3}, \tag{15}$$

$$T_e=1.0 \text{ eV}, \quad V=0 \text{ V}. \tag{16}$$

Tests using different initial conditions showed that the final results were independent of the choice of initial conditions.

In previous works[8–10] the electron-particle reaction rates were expressed as a function of electron temperature in an Arrhenius form. The goal of these earlier studies was to analyze the general features of electropositive discharges, rather than to simulate a specific discharge. The Arrhenius expressions, however, are not realistic for an argon discharge.

A different approach was followed in the present paper to obtain more realistic rate coefficients.[40] The Boltzmann transport equation was solved for an array of values of the electric field to neutral density ratio, E/N, to determine the eedf. The rate coefficients were then calculated from the known cross section $\sigma_j(\epsilon)$ for process $j$ using the expression

$$k_j=\int_0^\infty f(\epsilon)\sigma_j(\epsilon)u(\epsilon)d\epsilon, \tag{17}$$

where $u(\epsilon)$ is the electron velocity, and $\epsilon$ is the electron energy. The mean electron energy was also calculated as a function of E/N. Then the rate coefficients were expressed as a function of mean electron energy. Results are shown in Fig. 2. In practice, look up tables were used to interpolate the rate coefficients for use in the balance equations (1)–(3) and (7).

The above approach for calculating the reaction rate coefficients for use in the fluid model assumes that the eedf under rf conditions is similar to that under static (dc) conditions. Meijer *et al.*[32] scrutinized this assumption by

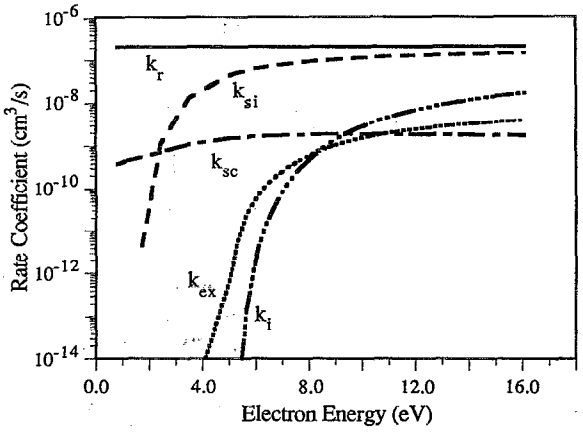


FIG. 2. Electron-neutral reaction rate coefficients as a function of electron energy. The meaning of $k$'s is given in Table I.

solving the Boltzmann equation in a space- and time-varying field similar to that found in an actual rf discharge between two parallel electrodes. They concluded that extrapolation of dc data to rf conditions is not permissible for evaluating the ionization rate coefficient as a function of E/N. However, they found that such extrapolation can be done provided that the ionization rate coefficient is expressed as a function of mean energy. Based on this finding, we expressed the reaction rate coefficients as a function of mean energy as shown in Fig. 2.

A more rigorous approach would be to abandon the electron density and energy (fluid) equations and solve the space- and time-dependent Boltzmann equation for the eedf (hybrid fluid-kinetic approach). However, it is not clear at the present time what level of sophistication should be incorporated into the model, in view of the fact that the excited-states chemistry is treated in an approximate manner. Hence it was decided to follow the simpler fluid-equations approach with rate coefficients as a function of mean energy in order to save computation time.

## III. METHOD OF SOLUTION

The problem consists of determining the electron, positive ion, and metastable atom density, electron energy, and potential as a function of space and time in the gap for a given set of system parameters. Electric field, current density, power dissipation, excitation, and ionization rates, and other derived quantities may then be obtained. The problem requires solution of the coupled system of parabolic [Eqs. (1), (2), (3), and (7)] and elliptic [Eq. (9)] partial differential equations (PDEs) subject to the appropriate boundary conditions [Eqs. (10)–(14)] and initial conditions [Eqs. (15) and (16)]. This system of PDEs was discretized in space by using the Galerkin finite element method.[41,42] The resulting differential/algebraic equation system (DAES) was solved by LSODI.[43,44] This routine uses a backward difference formula with automatically variable order and variable time-step size, controlled by estimating the time discretization error. Ninety linear elements were used with smaller element size near the electrodes where steep gradients are expected. The coordinates of the nodes $x_i$ ($i=1, N_p$) are given by the following formula:

$$x_i=\frac{L}{2}\left(\frac{i-1}{(N_p-1)/2}\right)^2 \quad i=1,(N_p-1)/2+1,$$

$$x_{N_{p-i+1}}=L-x_i \quad i=1,(N_p-1)/2+1,$$

where $L$ is the interelectrode spacing and $N_p$ is the number of nodes used ($N_p=91$). Increasing the number of elements to 120 had insignificant effect on the computed results.

The presence of metastables presented a problem due to the slow response time ($\sim 10$ ms) of the metastable density, $n_*$. Indeed, one must integrate for $\sim 10^5$ rf cycles for the metastable density to reach steady state. In order to avoid the tedious direct-time integration, an "acceleration" scheme was employed based on the Newton–Raphson method.[29,45]

Spatial discretization of the PDE system of interest leads to a system of the form $\mathbf{A}\dot{\phi}=\mathbf{F}$, the harmonic steady state of which we are seeking. Here $\mathbf{A}$ is the (known) stiffness matrix, $\phi$ is the vector of (unknown) dependent variables (e.g., metastable density), $\dot{\phi}$ is the time derivative of $\phi$, and $\mathbf{F}$ is the force vector which is a nonlinear function of the unknowns. At steady state, the values of each dependent variable must be identical at the start and end of the rf cycle,

$$\phi_0-\phi_1(\phi_0)=0. \tag{18}$$

Here subscripts 0 and 1 denote the value of the dependent variable at time $\tau$ and $\tau+\tau_{\rm rf}$, respectively, where $\tau_{\rm rf}$ is the rf period. Equation (18) consists of a system of nonlinear equations, with respect to the unknown vector $\phi_0$. This system can be solved by the classical Newton–Raphson method. An initial guess of $\phi_0$ is corrected according to

$$\phi_0^{\rm new}=\phi_0^{\rm old}-\Delta\phi_0, \tag{19}$$

where $\Delta\phi_0$ is calculated by solving the following system:

$$\mathbf{J}\Delta\phi_0=\phi_0-\phi_1. \tag{20}$$

The Jacobian $\mathbf{J}$ is

$$\mathbf{J}=\mathbf{I}-\left(\frac{\partial\phi}{\partial\phi_0}\right)_{\tau=1} \tag{21}$$

and matrix $(\partial\phi/\partial\phi_0)_{\tau=1}$ is computed by solving the following system of ODE's

$$\mathbf{A}\frac{d}{d\tau}\left(\frac{\partial\phi}{\partial\phi_0}\right)=\frac{\partial\mathbf{F}}{\partial\phi}\frac{\partial\phi}{\partial\phi_0}, \tag{22}$$

$$\frac{\partial\phi}{\partial\phi_0}=\mathbf{I}, \quad @\tau=0. \tag{23}$$

An example to illustrate the acceleration method is given in the Appendix.

In practice, the acceleration scheme was applied as follows: The complete system of Eqs. (1)–(9) was integrated directly for a number of rf cycles depending on the initial conditions. For the initial conditions given by Eqs. (14) and (15), integration proceeded for 50–100 rf cycles. Then, acceleration was applied on the metastable density equation (3). Following that, the system was allowed to relax by integrating the complete set of equations again for a number of rf cycles (usually $\sim 50$ cycles). This procedure was repeated several times until convergence. The convergence criterion was based on

$$\epsilon_{pss}=\left(\frac{\Sigma_{j=1}^{N_p}[(Q_j/Q_{\rm av})_{(I+1)\tau_{\rm rf}}-(Q_j/Q_{\rm av})_{I\tau_{\rm rf}}]^2}{N_p^2}\right)^{1/2}, \tag{24}$$

where $Q_j$ is the value of $Q$ at node $j$, $Q_{\rm av}$ is the spatially average value of $Q$, and $\epsilon_{pss}$ in a user-specified error tolerance. Convergence was declared when the following two criteria were satisfied: (a) The relative metastable density $\|\Delta\phi_0\|/\|\phi_0\|$ changed by less than 0.1% during the

TABLE III. Base case operating conditions.

| Name | Symbol | Base value |
|---|---|---|
| Gas density | $N$ ($cm^{-3}$) | $3.22\times10^{16}$ (1 Torr, 300 K) |
| Interelectrode spacing | $L$ (cm) | 2.54 |
| rf peak voltage | $V_{rf}$ (V) | 100 |
| rf frequency | $f$ (MHz) | 13.56 |

acceleration step, *and* (b) the electron and ion density, potential, and electron temperature were *all* required to satisfy Eq. (24) with $\epsilon_{pps}=10^{-5}$ for 10 consecutive rf cycles.

With the acceleration scheme, convergence of the complete system of equations was obtained with less than 1000 rf cycles. Without acceleration, one would need $\sim10^5$ rf cycles to achieve convergence. For a simulation including metastables the run time was $\sim1$ h on an Apollo 730 workstation. This puts two-dimensional computations including metastables within reach.

## IV. RESULTS AND DISCUSSION

Parameter values used for calculations are shown in Table III. The base values were: argon gas number density $N=3.22\times10^{16}$ (1 Torr, 300 K), excitation frequency $f=13.56$ MHz, electrode spacing $L=2.54$ cm, and peak rf voltage of 100 V (200 V peak-to-peak). Simulations for 50 and 75 V peak rf voltage were performed as well. Unless noted otherwise, conditions were at their base value (Table III). In the following, discharge properties are compared for two kinds of simulations for otherwise identical conditions: (a) in the simulation *including metastables* the complete system of Eqs. (1)–(9) was solved; (b) in the simulation *without metastables,* Eqs. (3) and (6) were dropped and coefficients $k_{si}$ and $k_{mp}$ were set equal to zero in Eqs. (1) and (2). Simulation results are summarized in Table IV. In the figures below, time $t$ was normalized with respect to the rf period ($\tau=ft$). Time $\tau=0$ corresponds to the positive zero crossing of the rf voltage applied to the left electrode, i.e., at time $\tau=0.25$ the left electrode is at its peak positive potential. Position between the two electrodes was normalized such that $\xi=0$ corresponds to the driven (left) electrode and $\xi=1$ corresponds to the grounded (right) electrode (Fig. 1).

Figure 3 shows the electron density distribution in the interelectrode space at four different times in the rf cycle including metastables [Fig. 3(a)] and without metastables [Fig. 3(b)]. The electron density is modulated substantially near the electrodes, with the electrons repelled by the momentary cathode ($\tau=0.75$, left electrode) and attracted by the momentary anode ($\tau=0.25$, left electrode). Electron density modulation in the bulk of the discharge is much weaker and cannot be resolved on the scale used for Fig. 3. The electron density is several times higher in the case including metastables. This is because of enhanced electron production by step-wise ionization and metastable pooling reactions. The higher electron density causes a thinner sheath when metastables are included. The calculated electron density compares well with the value of $\sim3\times10^{10}$ $cm^{-3}$ obtained experimentally under the same conditions (1 Torr, 100 V rf, 2.54 cm spacing) using microwave interferometry.[46]

The ion density (Fig. 4) is not modulated by the rf since the ions are too massive to respond to the rapidly changing field. The ion density is only slightly higher than the electron density in the bulk where quasi-neutrality is maintained. In contrast, the ion density is significantly higher than the electron density in the sheath region near the walls. The time-averaged electron (not shown) and positive ion profiles were symmetric since there was no dc bias between the equal area electrodes.

The metastable density profiles are shown in Fig. 5 for two values of the rf voltage. The peaks in metastable density near the plasma/sheath interface are due to (a) en-

TABLE IV. Summary of simulation results.

| | With metastables | | W/O metastables | |
|---|---|---|---|---|
| Applied peak potential $V_{rf}$ (V) | 50 | 100 | 50 | 100 |
| Current density $J_0$ ($mA/cm^2$) | 1.05 | 2.07 | 0.65 | 1.63 |
| Phase shift, total current vs voltage | 82.4° | 86.4° | 64.8° | 79.2° |
| Bulk electron "temperature" (eV) | 3.39 | 3.39 | 3.74 | 3.73 |
| | Space- and time-average quantities | | | |
| Electron density ($cm^{-3}$) | $7.36\times10^{9}$ | $1.52\times10^{10}$ | $1.26\times10^{9}$ | $3.28\times10^{9}$ |
| Positive ion density ($cm^{-3}$) | $7.46\times10^{9}$ | $1.54\times10^{10}$ | $1.33\times10^{9}$ | $3.41\times10^{9}$ |
| Metastable density ($cm^{-3}$) | $2.30\times10^{11}$ | $3.12\times10^{11}$ | ... | ... |
| Electron "temperature" (eV) | 3.50 | 3.61 | 3.86 | 4.01 |
| Potential (V) | 35.96 | 54.00 | 30.52 | 49.13 |
| Power dissipation ($mW/cm^3$) | 2.31 | 6.65 | 2.77 | 8.11 |
| $R_{ex}$ ($cm^{-3}\,s^{-1}$) | $6.06\times10^{14}$ | $1.38\times10^{15}$ | $1.24\times10^{15}$ | $3.13\times10^{15}$ |
| $R_r$ ($cm^{-3}\,s^{-1}$) | $3.38\times10^{14}$ | $8.64\times10^{14}$ | ... | ... |
| $R_{si}$ ($cm^{-3}\,s^{-1}$) | $7.54\times10^{13}$ | $1.90\times10^{14}$ | ... | ... |
| $R_{mp}$ ($cm^{-3}\,s^{-1}$) | $3.59\times10^{13}$ | $7.28\times10^{13}$ | ... | ... |
| $R_{3q}$ ($cm^{-3}\,s^{-1}$) | $2.62\times10^{13}$ | $3.56\times10^{13}$ | ... | ... |
| $R_{2q}$ ($cm^{-3}\,s^{-1}$) | $2.22\times10^{13}$ | $3.02\times10^{13}$ | ... | ... |
| $R_i$ ($cm^{-3}\,s^{-1}$) | $8.63\times10^{12}$ | $1.75\times10^{13}$ | $4.17\times10^{13}$ | $1.39\times10^{14}$ |
| $R_{sc}$ ($cm^{-3}\,s^{-1}$) | $2.51\times10^{12}$ | $6.30\times10^{12}$ | ... | ... |

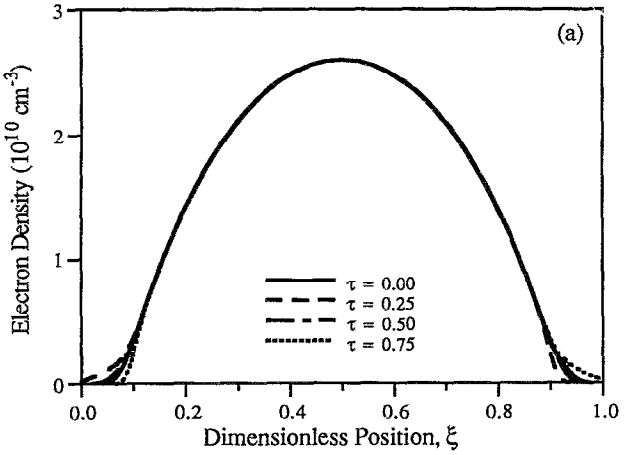


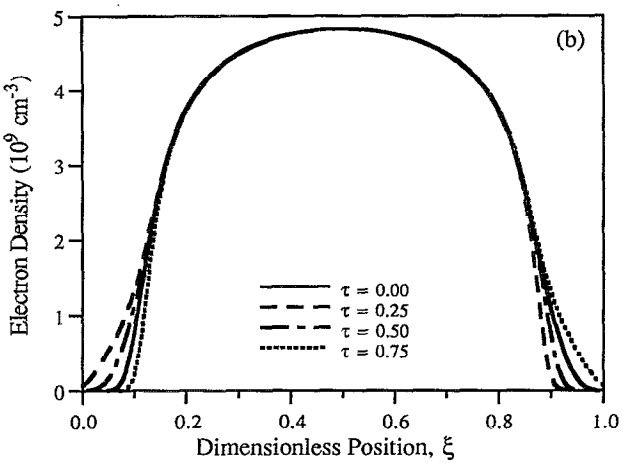


FIG. 3. Spatiotemporal variation of electron density: case (a) including metastables, case (b) without metastables. Conditions are the base values (Table III).

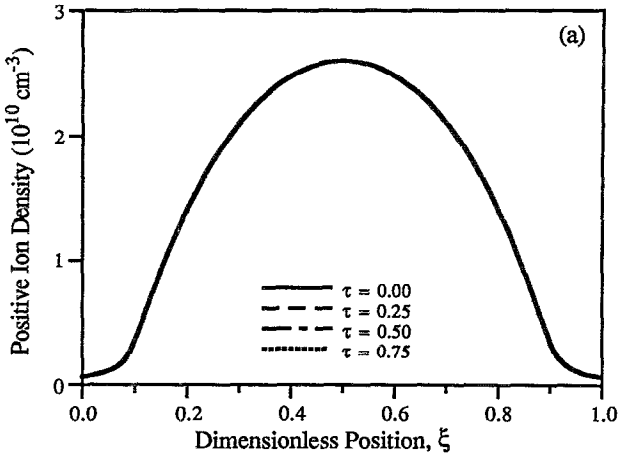


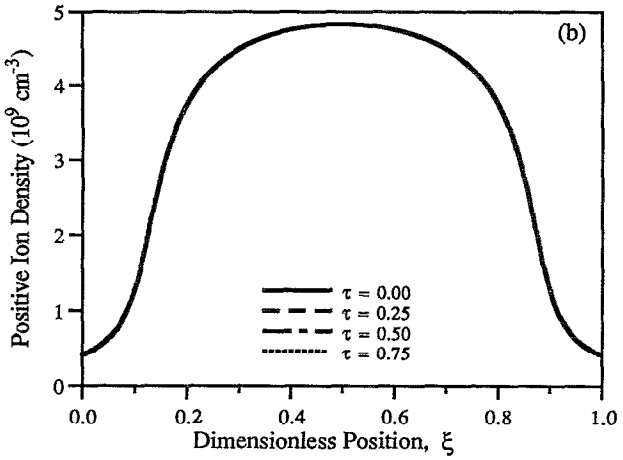


FIG. 4. Spatiotemporal variation of ion density: case (a) including metastables, case (b) without metastables. Conditions are the base values (Table III).

hanced production of metastables near the plasma/sheath interface due to higher electron energy (see Fig. 6) and (b) enhanced losses of metastables by electron quenching (reaction $R5$) in the central region of the discharge due to higher electron density there [Fig. 3(a)]. The metastable density peaks are at the same location as the peaks of the time-average excitation profiles (Fig. 10). The peak in metastable density is much reduced for 50 V rf voltage, since the electron energy around the plasma/sheath interface is then correspondingly lower. (Note that the *bulk* electron energy does not change significantly when going from 100 to 50 V peak rf voltage, and hence the production of metastables in the bulk remains unchanged.) Simulations using a peak rf voltage of 25 V showed very weak peaks in metastable density. The space-average metastable density is $3.12\times10^{11}$ cm$^{-3}$ for 100 V peak rf voltage decreasing to $2.30\times10^{11}$ cm$^{-3}$ when the applied peak rf voltage is made 50 V. The corresponding power density is 6.65 and 2.31 mW/cm$^3$, respectively (Table IV). One observes that the metastable density is only a weak function of power. This is because the metastable production rate as well as the main metastable loss rate (electron quenching, see below) are both proportional to electron density (which is nearly proportional to power). The metastable density was found to be a weak function of pressure as well (0.5–1.0 Torr). These results as are consistent with preliminary laser induced fluorescence (LIF) measurements of the $^3P_2$ metastable density in a parallel-plate discharge under comparable conditions.[40]

In order to assess the effect of any uncertainty of the excitation rate coefficient on the metastable density, a run was made setting $k_{ex}$ at 50% of the value shown in Fig. 2. The result is also shown in Fig. 5. The peaks in the metastable density profile are further reduced (compare curves at 50 V with $k_{ex}$ and $k_{ex}/2$).

Our results on metastable density profiles are in contrast to the findings of Makabe *et al.*[39] These authors obtained a metastable density profile corresponding to the fundamental diffusion mode with a maximum at the center. They concluded that loss of metastables is diffusion-

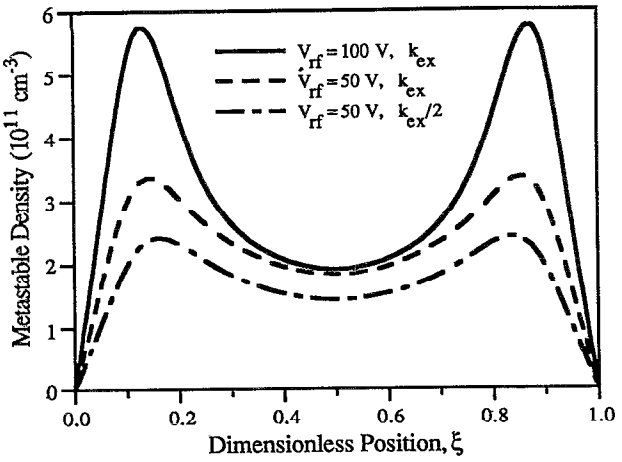


FIG. 5. Spatial variation of metastable density for two values of the peak rf voltage. Other conditions are the base values (Table III), except that dash-dotted curve was obtained using an excitation rate coefficient $k_{ex}$ 50% lower than the value given in Fig. 2. The metastable density is not modulated in time.

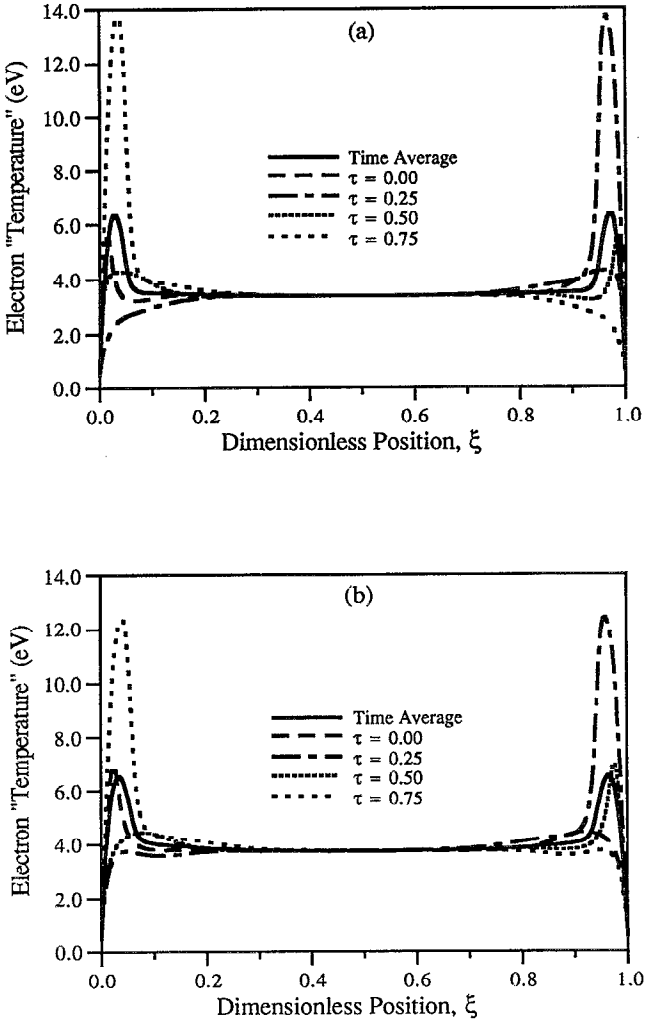


FIG. 6. Spatiotemporal variation of electron "temperature:" case (a) including metastables, case (b) without metastables. The time-averaged electron temperature is also shown. Conditions are the base values (Table III).

controlled. However, data reported in their paper suggest that diffusion is *not* the dominant loss process for metastables. They report a characteristic metastable diffusion time of 7.2 ms. In their Table II they also report a deactivation rate by electrons (corresponding to our $k_r$, Table I) of $1.8\times10^{-7}$ cm$^3$ s$^{-1}$ (average value). When this is multiplied by their electron density ($\approx3\times10^9$ cm$^{-3}$) and the product inverted, there results a characteristic reaction time of 1.85 ms, which is shorter than the diffusion time.

We found that electron quenching to the resonant state is the dominant loss process of metastables. Diffusion, step-wise ionization, metastable pooling, and two- and three-body quenching follow in order of importance. Superelastic collision losses of metastables are negligible. Peaks in metastable density near the plasma/sheath interface were observed experimentally by Scheller *et al.*[47] in a 50 kHz argon discharge. The metastable density measured by these authors at 0.3 Torr was $n_*\approx1.2\times10^{11}$ cm$^{-3}$.

The electron "temperature" distribution is shown in Fig. 6. The temperature peaks near the plasma-sheath interface and steep gradients develop in that region. Electrons which diffuse towards the electrode during the sheath potential minimum (around $\tau=0.25$ at left electrode, see also Fig. 3) are pushed back into the plasma as the potential reverses during the cathodic part of the cycle. One can think of electrons "riding the wave" as the sheath boundary moves away from the electrode during the cathodic part of the cycle. The electric field in the bulk plasma is much weaker than that in the sheath. Hence the bulk electron temperature is lower than that near the sheaths. The bulk electron temperature in the case including metastables is 3.39 eV (this corresponds to an energy of 5.09 eV), and is lower than the 3.73 eV bulk temperature of the case without metastables. This can be understood by examining the electron density balance. In the case with metastables, the major electron production mechanism is step-wise ionization. Other mechanisms include ionization of ground state atoms and metastable pooling. In the case without metastables, the only mechanism for electron production is ground state ionization. Since step-wise ionization has much lower threshold energy than ground state ionization (Table I), one can sustain the discharge with lower mean electron energy when metastables are present. (Actually, a metastable must be formed by excitation before it can be ionized. Hence, in the case with metastables, the electron energy in the discharge is controlled by the dependence of the excitation rate coefficient on energy, see Fig. 2.) The lower bulk electron energy when metastables are included can also be explained by looking at the bulk electric field (Fig. 7). The electric field amplitude is reduced with metastables present.

The ionization rate profiles of ground state atoms are shown in Fig. 8. In both cases (with or without metastables) the ionization rate peaks near the plasma/sheath interface, where electron energy is higher. Some background ionization of argon atoms is seen in the bulk of the plasma

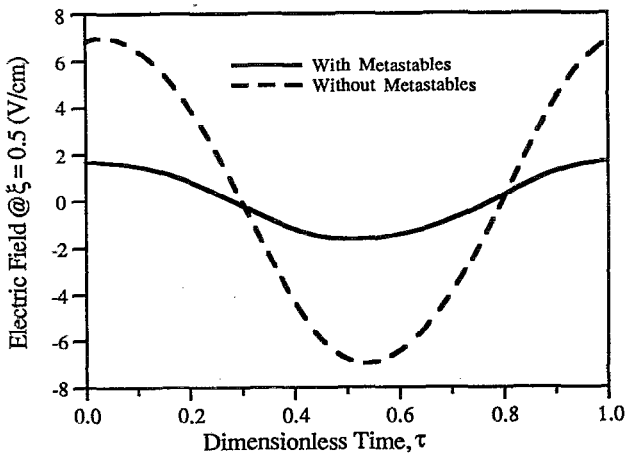


FIG. 7. Time modulation of the electric field at the discharge center. Conditions are the base values (Table III).

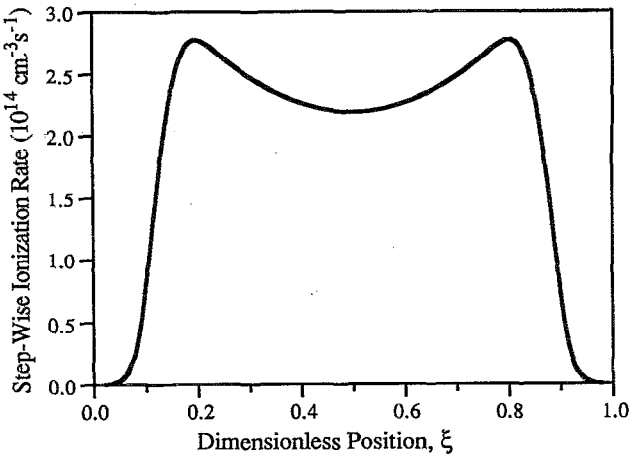


FIG. 9. Time-averaged distribution of step-wise (metastable) ionization rate. Conditions are the base values (Table III).

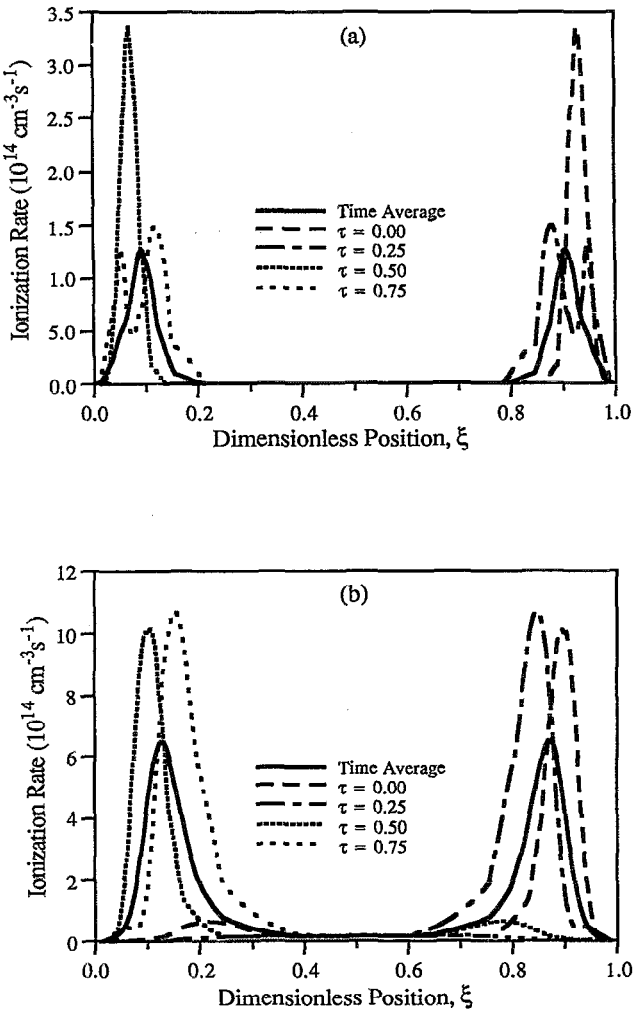


FIG. 8. Spatiotemporal variation of ionization rate: case (a) including metastables, case (b) without metastables. The time-averaged ionization rate is also shown. Conditions are the base values (Table III).

in the case without metastables [Fig. 8(b)], but this ceases when metastables are included. This is consistent with the lower bulk electric field and electron energy in the case including metastables. On a spatially averaged sense, ground state ionization is reduced by an order of magnitude when including metastables. In this case most of the ionization is provided by the step-wise process (Fig. 9). The importance of metastables and their effect on discharge maintenance are well established in the literature of the positive column of dc discharges.[48–50] Our results for the rf discharge also indicate that metastables must be included in the charged species balance [Eqs. (1) and (2)] to obtain a correct description of the discharge. Hence the assumption of Makabe *et al.*[39] neglecting step-wise ionization is not justified. The fractional density of metastables is only $\sim 10^{-5}$ yet these species play an important role in the discharge.

Step-wise ionization is a substantial source of electrons in the bulk plasma. Since the threshold of the step-wise process (4.14 eV) is much lower than that of direct ionization (15.7 eV) the bulk electric field need not be as high to sustain the discharge in the case including metastables (Fig. 7). The step-wise ionization rate profile is the product of the metastable density (Fig. 5), electron density (Fig. 3), and step-wise ionization coefficient profiles. The metastable density peaks near the plasma/sheath interface but the electron density is relatively low in that region. On the other hand, the metastable density is low near the center where the electron density peaks. Further, the electron energy and hence the step-wise ionization rate coefficient is almost constant throughout the bulk of the discharge. These features combine to yield the step-wise ionization profile shown in Fig. 9.

The excitation rate profiles are shown in Fig. 10. Substantial modulation is observed even deep in the bulk plasma. The excitation peak moves away from the left electrode and is washed into the bulk plasma as the left electrode potential goes through the negative zero crossing ($\tau = 0.5$), to the maximum negative potential ($t = 0.75$), to

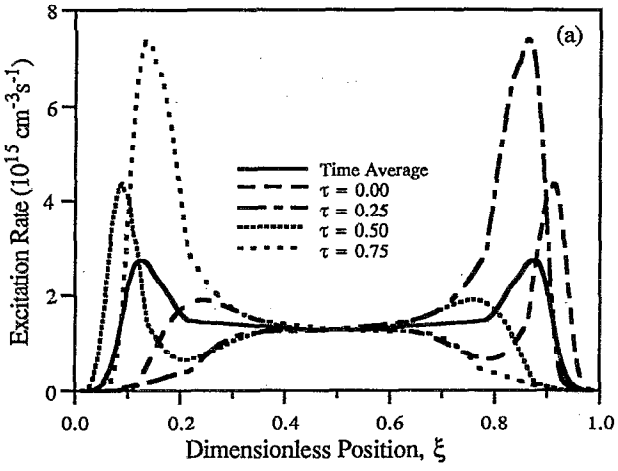


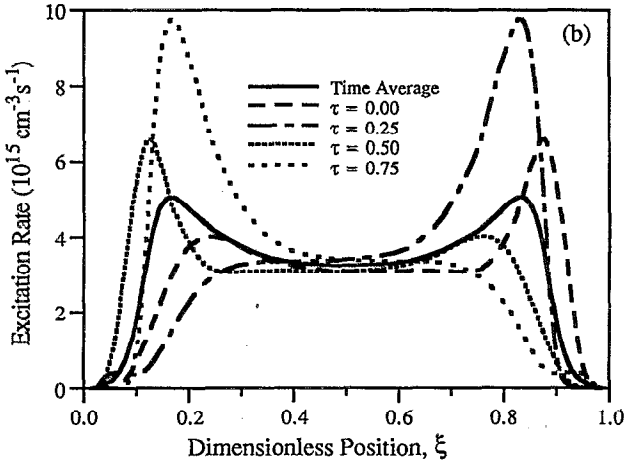


FIG. 10. Spatiotemporal variation of excitation rate: case (a) including metastables, case (b) without metastables. The time-averaged excitation rate is also shown. Conditions are the base values (Table III).

the positive zero crossing ($\tau$=0), and finally to the maximum positive potential ($\tau$=0.25). The situation at the right electrode is symmetric but 180° out of phase. The spatiotemporal variations of the excitation rate are shown more pictorially in Fig. 11.

The spatial dependence of the total power deposition is shown in Fig. 12. A greater fraction of the power is dissipated in the bulk plasma in the case without metastables, despite the fact that the electron density is lower without metastables. This is because the bulk electric field is much higher when metastables are not included (see Fig. 7) and this more than counterbalances the electron density effect. In both cases a significant fraction of the power is deposited near the sheaths. For 100 V peak rf voltage the space- and time-average power dissipation was 6.65 mW/cm$^3$ when including metastables and 8.11 mW/cm$^3$ without metastables. The phase shift between current and voltage waveforms was 86.4° and 79.2°, respectively. These results indicate that the discharge is primarily capacitive (due to the sheaths) with a resistive component (due to the bulk

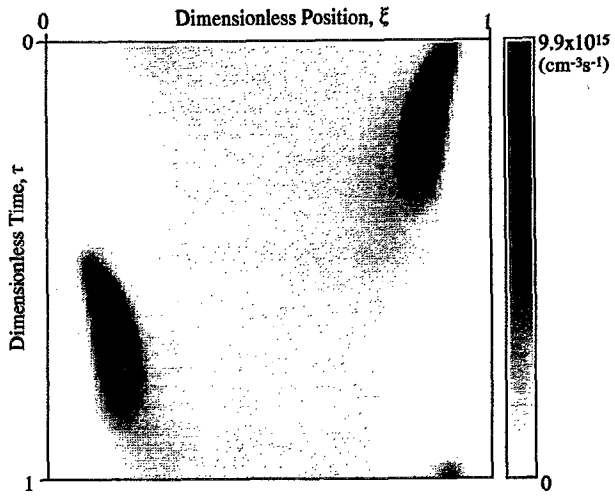


FIG. 11. Phase-space portrait of excitation rate. Conditions are the base values (Table III).

plasma). With metastables present the discharge shows more capacitive behavior (phase shift closer to 90°) compared to that without metastables. This is because the electron density is higher with metastables and this reduces the resistive component of the discharge.

## V. SUMMARY AND CONCLUSIONS

One-dimensional fluid simulations of a coupled glow-discharge/neutral-transport-reaction system were carried out in a parallel plate geometry with 13.56 MHz excitation. In particular, the effect of neutral metastable species in an argon glow discharge was studied. The simulation included balance equations for the density of electrons, positive ions, and metastable species, an equation for electron energy, as well as Poisson's equation to compute the self-consistent electric field. The partial differential equations were discretized in space using a finite element method and the resulting system of ordinary differential equations was in-

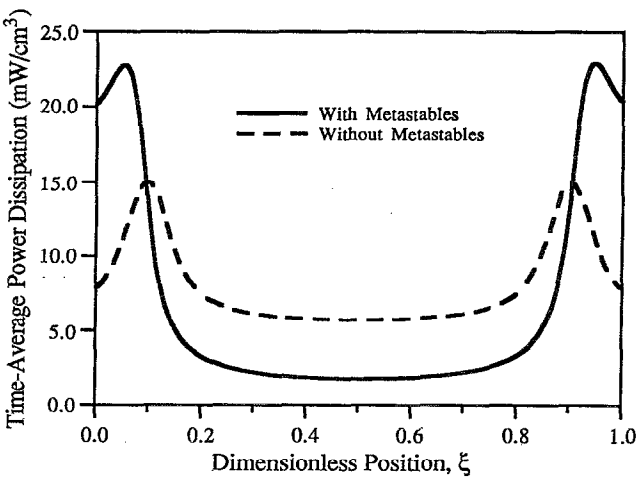


FIG. 12. Time-averaged power dissipation profiles. Conditions are the base values (Table III).

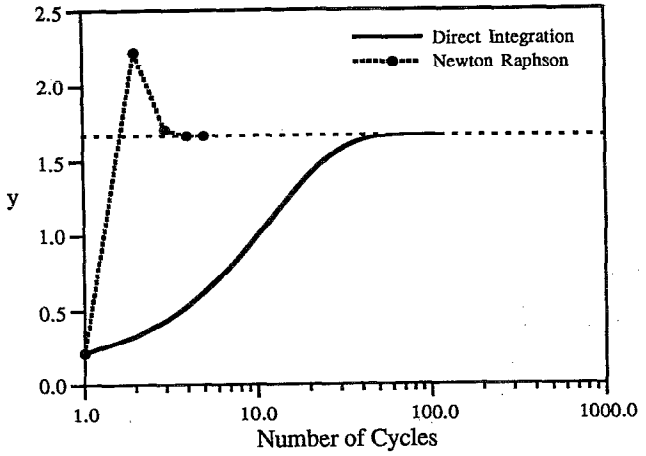


FIG. 13. Convergence behavior of Eq. (25). The time modulation of $y$ is not shown for clarity.

tegrated in time to obtain the periodic steady state. Due to the slow response time of neutral reactions ($\sim 10$ ms), direct time integration is tedious and requires $\sim 10^5$ rf cycles to converge. This translates to prohibitively long computation times. An "acceleration" technique based on the Newton–Raphson method was used to speed up computation of the periodic steady state, thereby reducing the computation time by orders of magnitude.

For a pressure of $\sim 1$ Torr, metastables were found to strongly influence the glow discharge. With metastables, step-wise ionization was the dominant mechanism of electron production overpowering direct ionization of ground state atoms, the latter being the only electron production mechanism in the discharge without metastables. For a constant applied voltage, the electron density was higher, bulk electron energy was lower, bulk electric field was lower, and phase shift between the current and voltage waveforms was closer to 90°, for the case including metastables as compared to the case without metastables. Also, the power deposition profiles were found to be quite different for the two cases. These results underscore the importance of metastable species despite the fact that their fractional density was lower than $10^{-5}$.

It was found that the metastable density profile has peaks near the glow/sheath interface. This was due to enhanced production of metastables in that region coupled with enhanced losses of metastables by electron quenching in the central region of the discharge. The peaks were reduced by decreasing the applied rf voltage because this also served to decrease the electron energy near the glow/sheath interface. The metastable density was predicted to be a weak function of power and pressure in accordance with preliminary LIF measurements. Currently, LIF measurements are being refined to obtain accurate values of metastable density as well as the spatial distribution of metastables.

The acceleration scheme is very useful for carrying out coupled glow-discharge/neutral-transport-reaction calculations of systems with complex plasma and neutral chemistry. This scheme is now being employed to carry out more detailed parametric investigations of the argon discharge including metastables and also to extend computations to two-dimensional geometries.

## ACKNOWLEDGMENTS

We are grateful to the State of Texas (Texas Advanced Research Program) and to the Welch Foundation for providing financial support. Thanks are also due to Professor Yannis Kevrekidis of Princeton University for helpful discussions.

## APPENDIX

To illustrate the effectiveness of the acceleration technique with a simple example, consider the following equation:

$$\frac{dy}{dt}=a\sin^2(\omega t)-by-cy^2. \tag{25}$$

This equation has the form of the metastable density balance: a source term modulated with twice the applied frequency, a linear loss term (corresponding, for example, to metastable quenching by electrons), and a quadratic loss term (corresponding to metastable pooling reactions). Equation (25) was solved for $a=0.25$, $b=0.05$, $c=0.015$, and $\omega=2\pi\ 13.56\times 10^6\ \mathrm{s}^{-1}$ using two methods: (a) direct time integration and (b) with the acceleration scheme. Figure 13 shows the value of $y$ at the end of each rf cycle versus the number of cycles (the actual modulation of $y$ is not shown for clarity). Direct integration requires $\sim 100$ rf cycles to reach the periodic steady state. The acceleration scheme converged after only a few cycles.

[1] S. M. Rossnagel, J. J. Cuomo, and W. D. Westwood, *Handbook of Plasma Processing Technology* (Noyes, Park Ridge, NJ, 1990).
[2] L. E. Kline and M. J. Kushner, Crit. Rev. Solid State Mater. Sci. **16**, 1 (1989).
[3] H. C. Wulu, K. C. Saraswat, and J. P. McVittie, J. Electrochem. Soc. **138**, 1831 (1991).
[4] E. S. Aydil and D. J. Economou, J. Electrochem. Soc. **139**, 1396 (1992).
[5] M. Dalvie and K. F. Jensen, J. Vac. Sci. Technol. A **8**, 1648 (1990).
[6] J. Kobayashi, N. Nakazato, and K. Hiratsuka, J. Electrochem. Soc. **136**, 1781 (1989).
[7] S. -K. Park and D. J. Economou, J. Electrochem. Soc. **137**, 2624 (1990).
[8] D. B. Graves and K. F. Jensen, IEEE Trans. Plasma Sci. **PS-14**, 78 (1986).
[9] D. B. Graves, J. Appl. Phys. **62**, 88 (1987).
[10] S. -K. Park and D. J. Economou, J. Appl. Phys. **68**, 3904 (1990); 4888 (1990).
[11] A. D. Richards, B. E. Thompson, and H. H. Sawin, Appl. Phys. Lett. **50**, 492 (1988).
[12] E. Gogolides, J. P. Nicolai, and H. H. Sawin, J. Vac. Sci. Technol. A **7**, 1001 (1989).
[13] J. -P. Boeuf and L. C. Pitchford, IEEE Trans. Plasma Sci. **19**, 286 (1991); J. -P. Boeuf, Phys. Rev. A **36**, 2782 (1987).
[14] S. Hashiguchi, J. Vac. Sci. Technol. A **10**, 1339 (1992).
[15] J. H. Tsai and C. Wu, Phys. Rev. A **41**, 5626 (1990).
[16] Y. Oh, N. Choi, and D. Choi, J. Appl. Phys. **67**, 3264 (1990).
[17] S. T. Pai, J. Appl. Phys. **71**, 5820 (1992); S. T. Pai and X. M. Guo, *ibid.* **71**, 5826 (1992).
[18] R. W. Boswell and I. J. Morey, Appl. Phys. Lett. **52**, 21 (1988).
[19] M. S. Barnes, T. J. Cotler, and M. E. Elta, J. Appl. Phys. **61**, 81 (1986); J. Comp. Phys. **77**, 53 (1988).

[20] R. W. Boswell and D. Vender, IEEE Trans. Plasma Sci. **19**, 141 (1991).
[21] M. Meyyappan, J. Appl. Phys. **69**, 8047 (1991); IEEE Trans. Plasma Sci. **19**, 122 (1991); J. Appl. Phys. **71**, 2574 (1992); M. Meyyappan and T. R. Govindan, J. Vac. Sci. Technol. A **10**, 1344 (1992).
[22] A. P. Paranjpe, J. P. McVittie, and S. A. Self, J. Vac. Sci. Technol. A **8**, 1654 (1990).
[23] G. R. Misium, A. M. Lichtenberg, and M. A. Lieberman, J. Vac. Sci. Technol. A **7**, 1007 (1989).
[24] W. Schmitt, W. E. Köhler, and H. Ruder, J. Appl. Phys. **71**, 5783 (1992).
[25] P. Mark and K. G. Müller, J. Appl. Phys. **70**, 6694 (1991).
[26] W. Nicholas, G. Hitchon, T. J. Sommerer, and J. E. Lawler, IEEE Trans. Plasma Sci. **19**, 113 (1991).
[27] V. A. Feoktistov, A. M. Popov, O. B. Popovicheva, A. T. Rakhimov, T. V. Rakhimova, and E. A. Volkova, IEEE Trans. Plasma Sci. **19**, 163 (1991).
[28] N. Sato and H. Tagashira, IEEE Trans. Plasma Sci. **19**, 102 (1991).
[29] E. Gogolides and H. H. Sawin, J. Appl. Phys. **72**, 3971 (1992); **72**, 3988 (1992).
[30] T. J. Sommerer and M. J. Kushner, J. Appl. Phys. **71**, 1654 (1992).
[31] C. Li and C. -H. Wu (unpublished).
[32] P. M. Meijer, W. J. Goedheer, and J. D. P. Passchier, Phys. Rev. A **45**, 1098 (1992).
[33] T. J. Sommerer, W. N. G. Hitchon, R. E. P. Harvey, and J. E. Lawler, Phys. Rev. A **43**, 4453 (1991).
[34] Y. A. Mankelevich, A. T. Rakhimov, and N. V. Suetin, IEEE Trans. Plasma Sci. **19**, 520 (1991).
[35] M. J. Kushner, J. Appl. Phys. **54**, 4958 (1983).
[36] R. K. Porteous and D. B. Graves, IEEE Trans. Plasma Sci. **19**, 204 (1991).
[37] M. Surendra and D. B. Graves, IEEE Trans. Plasma Sci. **19**, 144 (1991).
[38] C. K. Birdsall, IEEE Trans. Plasma Sci. **19**, 65 (1991).
[39] T. Makabe, N. Nakano, and Y. Yamaguchi, Phys. Rev. A **45**, 2520 (1992).
[40] N. L. Gronlund, Ph.D. thesis (in preparation) University of Houston.
[41] L. Lapidus and W. E. Schiesser, *Numerical Methods for Differential Systems* (Academic, New York, 1976).
[42] T. J. R. Hughes, *The Finite Element Method* (Prentice Hall, Englewood Cliffs, NJ, 1987).
[43] A. C. Hindmarsh, in *Scientific Computing,* edited by R. S. Stepleman (IMACS, North Holland, 1983), p. 55.
[44] A. C. Hindmarsh, Lawrence Livermore Lab. Report UCRL-87406 (1982) and UCRL-89311 (1983).
[45] Y. Kevrekidis, Ph. D. thesis, University of Minnesota, 1985; P. H. Strohband, R. Laur, and W. L. Engl, IEEE J. Solid-State Circuits SC-**12**, 243 (1977).
[46] K. Greenberg and G. A. Hebner (unpublished).
[47] G. R. Scheller, R. A. Gottscho, T. Intrator, and D. B. Graves, J. Appl. Phys. **64**, 4384 (1988).
[48] C. M. Ferreira, J. Loureiro, and A. Richards, J. Phys. D:Appl. Phys. **16**, 1611 (1983).
[49] C. M. Ferreira and J. Loureiro, J. Appl. Phys. **57**, 82 (1985).
[50] E. V. Karoulina and Yu A. Lebedev, J. Phys. D:Appl. Phys. **25**, 410 (1992).
[51] A. L. Ward, Phys. Rev. **112**, 1852 (1958).
[52] I. Yu Baranov, V. I. Demidov, and N. B. Kolokolov, Opt. Spectrosc. **51**, 316 (1981).